Chemical Physics Letters 748 (2020) 137337

Contents lists available at ScienceDirect

Chemical Physics Letters

journal homepage: www.elsevier.com/locate/cplett

Research paper

Local vibrational force constants – From the assessment of empirical force constants to the description of bonding in large systems

Wenli Zou[a], Yunwen Tao[b], Marek Freindorf[b], Dieter Cremer[c], Elfi Kraka[b,*]

[a] Institute of Modern Physics, Northwest University, and Shaanxi Key Laboratory for Theoretical Physics Frontiers, Xi'an, Shaanxi 710127, China
[b] Department of Chemistry, Southern Methodist University, 3215 Daniel Avenue, Dallas, TX 75275-0314, United States
[c] In Memoriam

HIGHLIGHTS

- Introduction of the local mode analysis as a powerful tool for the analysis of vibrational spectroscopy data.
- Assessment of the quality of empirically derived force constants.
- Detailed disclosure of bonding features in large molecules.
- Design of metal ligand force field parameters.

ARTICLE INFO

Keywords:
Local vibrational mode theory
Local mode force constants
Relaxed force constants
Bond strength measure
Metal ligand force field parameters

ABSTRACT

The local vibrational mode analysis, originally introduced by Konkoli and Cremer, provides a physically sound platform for a comprehensive analysis of calculated or measured vibrational spectra and for providing detailed insights into chemical bonding and other structural features. In this work, we summarize the essentials of the local vibrational mode theory with a focus on local vibrational force constants and their relationship with compliance and relaxed force constants. Furthermore, we discuss how local vibrational force constants can be used (i) to assess the quality of empirically derived force constants, (ii) to disclose bonding features in large molecules, and (iii) to provide metal ligand force field parameters. Future applications will be suggested.

1. Introduction

The idea of using stretching force constants as bond strength descriptors dates back to the 1930ies, when Badger discovered a force constant – bond length relationship for diatomic molecules [1]. However, the extension of the so-called Badger rule to polyatomic molecules turned out to be difficult, because spectroscopically derived stretching force constants are not unique. They depend on the internal coordinates used to describe the molecule and they reflect the coupling between the vibrational modes [2–4]. In the 1960ies, Decius introduced a solution of the force constant problem by reverting to the inverse force constant matrix, which he called *compliance matrix* [5]. He proved that the compliance matrix ($\mathbf{\Gamma}$) is independent of the choice of the internal coordinates used and that it is valid for redundant and non-redundant internal coordinate sets [5]. Based on these findings, he then suggested to use the diagonal elements Γ_{nn}, (the so-called *compliance constants*) as bond strength descriptors. However, Jones and Swanson pointed out that compliance constants connect a stronger chemical bond with a smaller force constant value, opposed to general chemical thinking [6]. Therefore, they introduced the reciprocal compliance constants $k_n^r = 1/\Gamma_{nn}$ as bond strength measure, which they called *relaxed force constants*, reflecting that according to Decius' definition [5] Γ_{nn} corresponds to the displacement of coordinate n resulting from a unit force imposed on coordinate n, while all other coordinates are allowed to relax to the minimum energy configuration with n being displaced [6]. Although frequently applied, the relationship between compliance/relaxed force constants and normal vibrational modes has remained unclear. Furthermore these are force constants without a corresponding mode, mass, frequency or intensity and they are lacking a physical basis. In addition, the interpretation of the reciprocal off-diagonal elements of the compliance matrix is difficult, because they can be either positive or negative. Absolute values have been used in same cases to describe strong and/or weak interactions [7].

In 1998, Konkoli and Cremer derived local vibrational modes utilizing a mass-decoupled equivalent of the Wilson equation of vibrational spectroscopy [8,9]. Their approach led to physically sound local

* Corresponding author.
E-mail address: ekraka@gmail.com (E. Kraka).

https://doi.org/10.1016/j.cplett.2020.137337
Received 18 January 2020; Received in revised form 6 March 2020; Accepted 9 March 2020
Available online 19 March 2020

mode force constants and related local mode properties. Furthermore, local vibrational modes can be uniquely transformed into the corresponding normal vibrational modes via an adiabatic connection scheme, thus enabling a detailed analysis of calculated or measured vibrational spectra via a decomposition of normal modes into local mode contributions [10,9]. Zou and Cremer demonstrated in a seminal paper that a local mode stretching force constant is directly related to the *intrinsic strength* of a bond, identifying local mode force constants as a unique measure of bond strength [11].

We summarize in this paper the local vibrational mode theory focusing on local mode force constants and their connection with compliance/relaxed force constants. We will then demonstrate how local mode force constants can be used to assess the quality of experimentally derived force constants, how they can serve as an efficient tool for the description of bonding in larger biochemical systems, and how they provide an attractive platform for the development of reliable metal-ligand force field parameters.

2. Methodology

In the following, the essence of the local vibrational mode theory will be presented including the definition of the local mode force constant, mass and vibrational frequency. The connection between local mode force constants and relaxed force constants will be discussed for stationary and non-stationary points on the potential energy surface. Finally, the computational methods used in this work will be summarized.

2.1. Theory of vibrational spectroscopy

For a vibrating molecule with K atoms, the Euler-Lagrange equations [3] can be written in Cartesian coordinates as

$$\mathbf{F}^x\mathbf{L} = \mathbf{ML\Lambda} \tag{1}$$

and also in internal coordinates

$$\mathbf{F}^q\mathbf{D} = \mathbf{G}^{-1}\mathbf{D\Lambda} \tag{2}$$

respectively, with the following connection between Eqs. (1) and 2)

$$\mathbf{F}^q = \mathbf{C}^\dagger\mathbf{F}^x\mathbf{C} \tag{3}$$

$$\mathbf{G} = \mathbf{BM}^{-1}\mathbf{B}^\dagger \tag{4}$$

$$\mathbf{D} = \mathbf{BL} \tag{5}$$

Generally, each normal mode $\mathbf{l}_\mu$ (a column vector of the **L** matrix with $\mu = 1, ...,N_{vib} = 3K - N_{tr}$, and $N_{tr} = 5$ or 6 for linear and non-linear molecules) is renormalized leading to the following relationships described in Eqs. (6) and 7) [12],

$$\mathbf{L}^\dagger\mathbf{F}^x\mathbf{L} = \mathbf{D}^\dagger\mathbf{F}^q\mathbf{D} = \mathbf{K} \tag{6}$$

$$\mathbf{L}^\dagger\mathbf{ML} = \mathbf{D}^\dagger\mathbf{G}^{-1}\mathbf{D} = \mathbf{M}^R \tag{7}$$

In Eqs. (1)–(7), $\mathbf{F}^x$ and $\mathbf{F}^q$ are the force constant (Hessian) matrices in Cartesian and internal coordinates, respectively, **L** collects the vibrational eigenvectors $\mathbf{l}_\mu$, **M** is the diagonal mass matrix of the molecule in question, matrix **K** is the diagonal force constant matrix in normal coordinates Q and matrices **B** and **G** are the Wilson **B** and **G** matrices [3]. Matrix **D** collects the normal mode vectors $\mathbf{d}_\mu$ in internal coordinates q. The eigenvalue matrix $\mathbf{\Lambda}$ is a diagonal matrix containing the vibrational eigenvalues

$$\lambda_\mu = K_\mu/M_\mu^R = 4\pi^2c^2\omega_\mu^2 \tag{8}$$

where ω_μ represents the (harmonic) vibrational frequency of the μ-th mode and c is the speed of light. The elements of **B** are defined by the partial derivatives of internal coordinates with regard to Cartesian coordinates [3], and **C** is the general-inverse of **B** defined by

$$\mathbf{C} = \mathbf{WB}^\dagger(\mathbf{BWB}^\dagger)^{-1} \tag{9}$$

where **W** is an arbitrary nonsingular $3K\times3K$ square matrix. Since the N_{tr} translational and rotational eigenvectors are decoupled from the N_{vib} vibrational eigenvectors at a stationary point (*i. e.*, the energy gradient is a zero-vector), **W** does not affect the results [13]. For reasons of simplicity, one often uses $\mathbf{W} = \mathbf{I}_{3K}$ (usually for a geometry optimization in internal coordinates) or $\mathbf{W} = \mathbf{M}^{-1}$. In vibrational spectroscopy, the latter definition is adopted in most of cases, thus leading to

$$\mathbf{C} = \mathbf{M}^{-1}\mathbf{B}^\dagger\mathbf{G}^{-1} \tag{10}$$

and then

$$\mathbf{BC} = \mathbf{I}_{\mathbf{Nvib}} \tag{11}$$

It has to be noted that $\mathbf{CB} \neq \mathbf{I}_{3K}$ since **B** is spanned in the N_{vib}-dimensional vibrational space only.

2.2. Local vibrational modes and related local mode properties

Konkoli and Cremer derived the local vibrational modes $\mathbf{a}_i$ directly from the normal vibrational modes bypassing the use of an inverted Hessian matrix [14,8]. As shown in Eq. (12), all what is needed are the diagonal force constant matrix **K** and the normal mode row vector $\mathbf{d}_i$ to define the i-th local mode being associated with the coordinate q_i

$$\mathbf{a}_i = \frac{\mathbf{K}^{-1}\mathbf{d}_i^\dagger}{\mathbf{d}_i\mathbf{K}^{-1}\mathbf{d}_i^\dagger} \tag{12}$$

where $\mathbf{d}_i$ is the i-th row vector of **D** in Eq. (5)

$$\mathbf{d}_i = \mathbf{b}_i\mathbf{L}, \tag{13}$$

The corresponding local force constant k_i^a of local mode i (superscript a denotes an adiabatically relaxed, i.e., local mode) can be expressed as

$$k_i^a = \mathbf{a}_i^\dagger\mathbf{K}\mathbf{a}_i. \tag{14}$$

After some algebra [10], Eq. (14) becomes

$$k_i^a = \frac{1}{\mathbf{d}_i\mathbf{K}^{-1}\mathbf{d}_i^\dagger} = \frac{1}{\mathbf{b}_i(\mathbf{LK}^{-1}\mathbf{L}^\dagger)\mathbf{b}_i^\dagger}. \tag{15}$$

In contrast to the procedure of Decius extracting compliance constants directly from $\mathbf{\Gamma} = (\mathbf{F}^q)^{-1}$, our local vibrational mode method has several important advantages: (1) the i-th local mode force constant depends only on the i-th local mode through its **B**-matrix vector $\mathbf{b}_i$, (2) the condition that the number of local mode parameters must be at least N_{vib} to construct the $\mathbf{F}^q$ is not necessary, and (3) most important, after Eq. (1) being solved by a quantum chemistry program, the calculation of the inverse of $\mathbf{F}^q$ as well as a diagonalization is not needed (the inverse calculation of the diagonal matrix **K** is easy), which makes our approach attractive for large molecules. In contrast, the calculation of compliance/relaxed force constants requires an additional calculation of either the inverse of $\mathbf{F}^q$ in the original definition [6] or the general-inverse of $\mathbf{F}^x$, as discussed below.

It should be noted that the units of the **B**-matrices for bond lengths and bond angles are different, and therefore in Eq. (15) the unit of a force constant for a bond angle is mDyn·Å(or mDyn·Å/rad^2). In early references, the force constant of a bond angle $\angle ABC$ was defined by [3,4]

$$\widetilde{k}_{\angle ABC} = k_{\angle ABC}\cdot r_{AB}^{-1}\cdot r_{BC}^{-1}. \tag{16}$$

Consequently, the unit of $\widetilde{k}_{\angle ABC}$ becomes mDyn/Å, i.e. the unit of a bond length. The same is also true for other angles like dihedral angles and curvilinear phase angles [15].

In addition to the local mode force constant, the local mode mass has also been derived from the **G** matrix [14,8],

$$m_i^a = 1/G_{i,i} = \frac{1}{\mathbf{b}_i\mathbf{M}^{-1}\mathbf{b}_i^\dagger}. \tag{17}$$

For a chemical bond A-B, Eq. (17) leads to $M_AM_B/(M_A + M_B)$, being the

same as the reduced mass of a diatomic molecule AB.

Inspired by Eq. (15), one may consider the following formula for the local mode mass

$$m_i^a = \frac{1}{\mathbf{d}_i(\mathbf{M}^R)^{-1}\mathbf{d}_i^\dagger} = \frac{1}{\mathbf{b}_i[\mathbf{L}(\mathbf{M}^R)^{-1}\mathbf{L}^\dagger]\mathbf{b}_i^\dagger} \tag{18}$$

In fact, Eqs. (17) and (18) are equivalent. To prove this, we define the augmented normal mode matrix $\overline{\mathbf{L}} = (\mathbf{L} \;\; \mathbf{L}_{tr})$ and $\mathbf{M}_{tr}^R = \mathbf{L}_{tr}^\dagger \mathbf{M} \mathbf{L}_{tr}$, where $\mathbf{L}_{tr}$ collects N_{tr} translational and rotational modes with the corresponding reduced mass matrix $\mathbf{M}_{tr}^R$. $\overline{\mathbf{L}}$ is a non-singular square matrix which is inversible, thus the denominator of Eq. (17) is

$$\begin{aligned}\mathbf{b}_i\mathbf{M}^{-1}\mathbf{b}_i^\dagger &= \mathbf{b}_i\overline{\mathbf{L}}(\overline{\mathbf{L}}^\dagger\mathbf{M}\overline{\mathbf{L}})^{-1}\overline{\mathbf{L}}^\dagger\mathbf{b}_i^\dagger \\ &= \mathbf{b}_i(\mathbf{L} \;\; \mathbf{L}_{tr})\begin{pmatrix}(\mathbf{M}^R)^{-1} & \mathbf{0} \\ \mathbf{0} & (\mathbf{M}_{tr}^R)^{-1}\end{pmatrix}\begin{pmatrix}\mathbf{L}^\dagger \\ \mathbf{L}_{tr}^\dagger\end{pmatrix}\mathbf{b}_i^\dagger \\ &= \mathbf{b}_i[\mathbf{L}(\mathbf{M}^R)^{-1}\mathbf{L}^\dagger]\mathbf{b}_i^\dagger + \mathbf{b}_i[\mathbf{L}_{tr}(\mathbf{M}_{tr}^R)^{-1}\mathbf{L}_{tr}^\dagger]\mathbf{b}_i^\dagger\end{aligned} \tag{19}$$

$\mathbf{b}_i\mathbf{L}_{tr} \equiv \mathbf{0}$ since $\mathbf{b}_i$ and $\mathbf{L}_{tr}$ are in the vibrational and translational-rotational spaces, respectively. Therefore the last term in Eq. (19) vanishes, indicating the equivalence of the two definitions of the local mode mass. In this work we use Eq. (17) instead of Eq. (18) for reasons of simplicity.

From the local mode force constant k_i^a and local mode mass m_i^a the local mode frequency ω_i^a can be calculated

$$(\omega_i^a)^2 = 1/\left(4\pi^2c^2\right)\frac{k_i^a}{m_i^a} = 1/\left(4\pi^2c^2\right)G_{ii}\mathbf{a}_i^\dagger\mathbf{K}\mathbf{a}_i \tag{20}$$

In addition, the local mode infrared intensity has been defined [12], which can be related to bond dipole moments [16–18]. In Fig. 1 the work flow of the local mode analysis is summarized in the form of a pseudocode.

2.3. Relaxed force constant vs. local mode force constant

It has been proved that k_i^a in Eq. (15) equals exactly the reciprocal of the i-th compliance constant, i.e. the relaxed force constant k_i^r, which will be outlined in the following [13]. The relaxed force constants can be expressed in terms of Cartesian coordinates [7] via

$$\mathbf{\Gamma} = \mathbf{B}(\mathbf{F}^x)^{\bar{1}}\mathbf{B}^\dagger \tag{21}$$

where $\bar{1}$ means the general-inverse of a singular matrix. Based on Eq. (21) the relaxed force constant of the i-th internal coordinate (k_i^r) can be calculated by

$$k_i^r = 1/\Gamma_{i,i} = \frac{1}{\mathbf{b}_i(\mathbf{F}^x)^{\bar{1}}\mathbf{b}_i^\dagger} \tag{22}$$

Using the augmented normal mode matrix $\overline{\mathbf{L}}$ defined above (the dimension of $\overline{\mathbf{L}}$ is $3K$ x $3K$, i.e. N_{vib} vibrations and N_{tr} rotations, translations), Eq. (6) becomes

$$\begin{pmatrix}\mathbf{K} & \mathbf{0} \\ \mathbf{0} & \mathbf{K}_{tr}\end{pmatrix} = \overline{\mathbf{L}}^\dagger\mathbf{F}^x\overline{\mathbf{L}} \tag{23}$$

where $\mathbf{K}_{tr}$ are the eigenvalues of the translational and rotational modes (usually zero or small). This leads to

$$(\mathbf{F}^x)^{\bar{1}} = \left[(\overline{\mathbf{L}}^{-1})^\dagger\begin{pmatrix}\mathbf{K} & \mathbf{0} \\ \mathbf{0} & \mathbf{K}_{tr}\end{pmatrix}\overline{\mathbf{L}}^{-1}\right]^{\bar{1}} \tag{24}$$

$$= \overline{\mathbf{L}}\begin{pmatrix}\mathbf{K} & \mathbf{0} \\ \mathbf{0} & \mathbf{K}_{tr}\end{pmatrix}^{\bar{1}}\overline{\mathbf{L}}^\dagger \tag{25}$$

Since $(K_{tr})_\mu = 0$ ($\mu = 1, 2, ..., N_{tr}$) at a stationary point, Eqs. (24) and (25) can be rewritten as

$$(\mathbf{F}^x)^{\bar{1}} = (\mathbf{L} \;\; \mathbf{L}_{tr})\begin{pmatrix}\mathbf{K}^{-1} & \mathbf{0} \\ \mathbf{0} & \mathbf{0}\end{pmatrix}\begin{pmatrix}\mathbf{L}^\dagger \\ \mathbf{L}_{tr}^\dagger\end{pmatrix} = \mathbf{L}\mathbf{K}^{-1}\mathbf{L}^\dagger \tag{26}$$

Inserting Eq. (26) into Eq. (22), it can be easily seen that k_i^r defined by Eq. (22) is exactly k_i^a via Eq. (15). Therefore, the relaxed force constant at a stationary point is equivalent to the adiabatic local mode force constant, and this is also true for the relaxed and adiabatic *coupling constants* between two internal coordinates.

At a non-stationary point (e.g. as caused by an inaccurate geometry optimization), the relaxed and adiabatic local mode force constants may differ to some extend. In the former method the gradients of internal coordinates have to be projected out from Hessian through the first-order derivatives of the **B**-matrix [19]. In our method, contributions from the translational and rotational modes are projected out from the Hessian when solving Eq. (1), that is, using the Eckart-Sayvetz conditions to generate N_{tr} translational and rotational vectors and the Gram-Schmidt orthogonalization for the rest N_{vib} vectors in the vibrational space [20], which have been implemented in most of the modern quantum chemistry programs including GAUSSIAN, GAMESS, or MOLPRO. This procedure is more robust and efficient.

1. Read data from a vibrational frequency calculation
   - Atomic masses and Cartesian coordinates
   - Hessian matrix $\mathbf{F}^x$
   - Normal modes $\mathbf{L}$ (*optional*)
   - Other data (*optional; not relevant to this work*)
2. Vibrational frequencies from experiments (*optional*)
3. If $\mathbf{L}$ is not available
   Solve the secular equation $\mathbf{F}^x\,\mathbf{L} = \mathbf{M}\,\mathbf{L}\,\mathbf{\Lambda}$
   End if
4. Read internal coordinates provided by the user, or generate redundant internal coordinates
5. Calculate Wilson's B-matrix of internal coordinates from Cartesian coordinates
6. $\mathbf{K} = \mathbf{L}^\dagger\mathbf{F}^x\mathbf{L}$
7. Do loop: for the i-th internal coordinate
   $\mathbf{d}_i = \mathbf{b}_i\mathbf{L}$
   $k_i^a = \left(\mathbf{d}_i\mathbf{K}^{-1}\mathbf{d}_i^\dagger\right)^{-1}$
   $m_i^a = \left(\mathbf{b}_i\mathbf{M}^{-1}\mathbf{b}_i^\dagger\right)^{-1}$
   $\omega_i^a = \sqrt{k_i^a/m_i^a}/(2\pi c)$
   End do
8. Other analysis

Fig. 1. Pseudocode of the local mode analysis.

2.4. Computational methods

CCSD(T) (coupled cluster with all single and double excitations and a perturbative treatment of triple excitations) [21] calculations were performed with the program package CFOUR [22], which provides analytic gradients [23] and analytic second derivaties [24]; DFT (Density Functional Theory) calculations were performed using the GAUSSIAN16 program package [25], whereas the local mode analysis was done using the COLOGNE19 program package [26]. All basis sets used in this work are taken from EMSL Basis Set Exchange [27,28]. The QM/MM calculations were performed with GAUSSIAN16 applying the ONIOM methodology [29], and using the AMBER force field [30] for the MM part.

3. Results and discussion

3.1. Assessment of experimentally derived vibrational force constants

The calculation of force constants and associated force fields from

Table 1
Comparison of local mode force constants by CCSD(T)/aug-cc-pVTZ with the experimental ones.

Molecule	Bond	k (mDyn/Å)			Angle	$\tilde{k}$ (mDyn/Å)		
		Expt.[(a)]	Expt.[(b)]	k^a		Expt.[(a)]	Expt.[(b)]	$\tilde{k}^a$
H_2O	H−O	7.8	8.43	8.260	H-O-H	0.69	0.77	0.746
H_2S	H−S	4.3	4.28	4.249	H-S-H	0.43	0.43	0.418
H_2Se	H−Se	3.3		3.491				
NH_3	H−N	6.5		6.798	H-N-H	0.50 [c)]		0.575
PH_3	H−P	3.1		3.331	H-P-H	0.33		0.342
AsH_3	H−As	2.6		3.138				
C_2H_4	H−C	5.1		5.541	H-C-H	0.30		0.593
	C−C	9.7 [c)]		9.135				
C_6H_6	H−C	5.1		5.558				
	C−C	7.6		6.393				
C_2H_2	H−C	5.9		6.337	H-C-C	0.12		0.158
	C−C	16.3 [c)]		16.100				
SiH_4	H−Si	2.9		2.903				
F_2O	F−O	5.6		3.987	F-O-F	0.69		0.729
Cl_2O	Cl−O	4.9		2.885	Cl-O-Cl	0.41		0.400
CH_3F	F−C	5.6		5.107	H-C-F	0.57		0.654
CH_3Cl	Cl−C	3.4		3.068	H-C-Cl	0.36		0.415
CH_3Br	Br−C	2.8		2.649	H-C-Br	0.30		0.413
CH_3I	I−C	2.3		2.328	H-C-I	0.23		0.321
BF_3	F−B	8.8	7.27	7.220	F-B-F	0.37	0.52	0.730
BCl_3	Cl−B	4.6	4.02	3.610	Cl-B-Cl	0.16	0.18	0.351
BBr_3	Br−B	3.7		3.009	Br-B-Br	0.13		0.301
P_4	P−P	2.1	2.06	2.009				
Si_2H_6	Si−Si	1.7		1.725				
S_2H_2	S−S	2.5		2.469				
$B_3N_3H_6$	B−N	6.3		5.421				
N_2O	N−N		17.88	17.924	N-N-O	0.49	0.49	0.493
	N−O	11.5	11.39	11.686				
CH_4					H-C-H	0.46		0.555
CF_4					F-C-F	0.71		0.993
CCl_4					Cl-C-Cl	0.33		0.434
CBr_4					Br-C-Br	0.24		0.381
CO_2	C−O		15.5	15.613	O-C-O	0.57	0.57	0.567
CS_2	C−S		7.5	7.674	S-C-S	0.23	0.23	0.229
HCN	H−C		5.7	6.214	H-C-N	0.20	0.20	0.205
	C−N		18.6	18.335				

[(a)] Experimental values from Tables 8–1 and 8–2 and in Ref. [3]
[(b)] Experimental values from Table 8–3 in Ref. [3].
[(c)] Averaged experimental value.

experimental frequencies goes back to the early 50ies. For example, in their famous vibrational spectroscopy book, Wilson, Decius, and Cross [3] discuss experimentally derived stretching and bending force constants for a selection of small molecules, collected in Tables 8–1,8–2, page 175 and 176 of Ref. [3] (labelled as *Series a* in this work), and Table 8–3, page 178 of Ref. [3] (labeled as *Series b* in this work). *Series a* force constants were obtained via a simple valence force function approach using a fourth-power potential function [31], whereas for *Series b* interactions between force constants were also taken into account [32]. We used these data as a test set to explore how the local mode force constants can be used to assess the quality of empirically derived force constants, in particular to disclose potential shortcomings. For this purpose we calculated the corresponding local mode force constants for these compounds at the CCSD(T)/aug-cc-pVTZ level, (for C_6H_6 cc-pVTZ was used). The results are shown in Table 1 and in Fig. 2. Experimental and calculated normal mode frequencies are provided as supplementary data. Local bending force constants $k^a_{\angle ABC}$ were converted to mDyn/Åunits to match the unit of the experimentally derived bending force constants.

As revealed by the data in Table 1 and Fig. 2, the agreement between local mode and empirical stretching force constants for *Series a* molecules is fairly good, (R^2 = 0.955; standard deviation: 0.74 mDyn/Å) and even better for *Series b* molecules, (R^2 = 0.997; standard deviation: 0.25 mDyn/Å). This shows that the valence force function approach, in particular considering interactions terms works well for estimating stretching force constants for the small molecules investigated in this work. This is no longer the case for the bending angles. The overall correlation of local mode and empirical bending force constants for *Series a* is poor as revealed by Fig. 2 (b) with the general trend that the empirical bending force constants become too small. If for *Series b* the two outliers BF_3 (local mode 0.73 *vs.* empirical 0.52 mDyn/Åfor F-B-F) and BCl_3(local mode 0.35 *vs.* empirical 0.18 mDyn/Åfor Cl-B-Cl) are excluded, the correlation between local mode and empirical force constants becomes significant. However, it has to be noted that the remaining data set is small and only composed of triatomic molecules. The empirical fitting function does no longer work for planar BF_3 and BCl_3 with D_{3h} symmetry. The decomposition of normal modes into local mode contributions can serve in this case as a helpful tool to retrieve more detailed information. As shown by Zou and coworkers, local mode frequencies are uniquely connected to their normal mode counterparts via an adiabatic connection scheme [10], which forms the fundamental basis for this decomposition, the characterization of normal mode (CNM) procedure [9].

CNM decomposes each normal vibrational mode $\mathbf{l}_\mu$ into local mode contributions for a non-redundant set of N_{vib} local vibrational modes $\mathbf{a_n}$ based on the overlap between each local mode vector $\mathbf{a}^x_n$ in Cartesian coordinates and the normal mode vector $\mathbf{l}_\mu$ as $S_{n\mu}$ according to Eq. (27) [33,9,34]

$$S_{n\mu} = \frac{(\mathbf{a}^x_n, \mathbf{l}_\mu)^2}{(\mathbf{a}^x_n, \mathbf{a}^x_n)(\mathbf{l}_\mu, \mathbf{l}_\mu)} \quad (27)$$

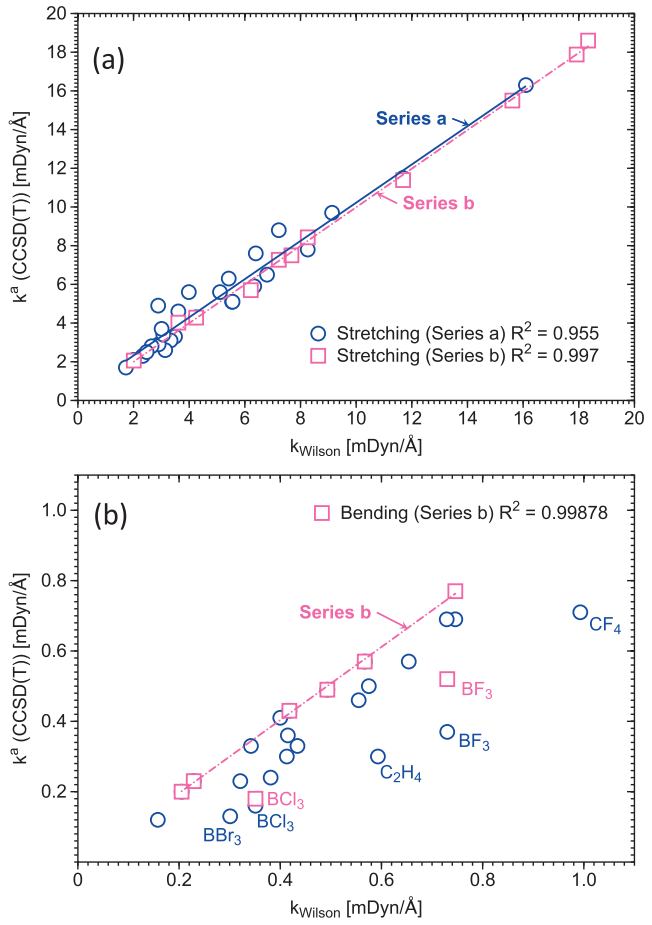

Fig. 2. Correlation between local mode force constants k^a based on the CCSD (T)/aug-cc-pVTZ level of theory and experimentally derived force constants k_{Wilson}. Fig. 2 (a) displays stretching force constants. Blue circles (*Series a*): experimental stretching force constant values taken from Tables 8–1 and 8–2 of Ref. [3]; Pink squares (*Series b*): experimental stretching force constant values taken from Table 8–3 of Ref. [3]. Fig. 2 (b) displays the corresponding bending force constants. BF_3 and BCl_3 were excluded from the fit.

$\mathbf{a}_n^x$ is the local mode vector in Cartesian coordinate space obtained via

$$\mathbf{a}_n^x = \mathbf{L}\mathbf{a}_n \tag{28}$$

where **L** is the normal mode matrix in Cartesian coordinates. (**a**, **b**) is the short notation for the scalar product two vectors of **a** and **b** including a metric

$$\left(\mathbf{a}, \mathbf{b}\right) = \sum_{i,j} a_i O_{ij} b_j \tag{29}$$

O_{ij} is an element of the metric matrix **O**. We generally use the force constant matrix $\mathbf{F}^x$ as metric, namely $\mathbf{O} = \mathbf{F}^x$, to include the influence of the electronic structure. As derived by Konkoli and Cremer [33] the contribution of local mode $\mathbf{a}_n$ to normal mode $\mathbf{l}_\mu$ is given by

$$C_{n\mu} = \frac{S_{n\mu}}{\sum_m^{N_{vib}} S_{m\mu}} \tag{30}$$

i.e. a completely localized normal mode $\mathbf{l}_\mu$ has a $C_{n\mu}$ value of 1 (corresponding to 100 % if $C_{n\mu}$ is given as percentage)

Fig. 3 (a) shows the CNM analysis for BF_3 and Fig. 3 (b) for C_2H_4, respectively. As reflected by Fig. 3 (a), the FBF angles dominate the degenerate E' modes at 477 cm^{-1} with almost 96 %, i.e. these modes have almost pure bending character. It is interesting to note is that bending angles also contributes with more than 10% to the degenerate E' stretching modes at 1473 cm^{-1}. In the case of C_2H_4 shown in Fig. 3 (b), the HCH bond angles equally contribute to the B_{1u} mode at 1472 cm^{-1} with 50%, identifying this mode as pure HCH bending mode. In addition the A_g mode at 1365 cm^{-1} has also 60% HCH character, whereas 40% results from CC bond stretching, for the A_g mode at 1666 cm^{-1} the situation is reversed, 60 % CC bond stretching and 40% HCH bending character. This complex interplay of the stretching and bending modes can no longer be covered by a simple valence force function approach.

3.2. Local mode force constants for the characterization of bonding in proteins

As a pilot study for the characterization of bonding in proteins with local mode force constants, we investigated the binding of azanone (HNO) to the heme group of myoglobin. Azanone has recently received attention because of its novel physiological or pharmacological properties, in particular when interacting with a metalloprotein [36]. Utilizing NMR, resonance Raman, and X-ray absorption spectroscopy, a stable complex of HNO and myoglobin was identified, involving the distal histidine of the heme pocket as proton donor (ε protonation state, see Fig. 4 [37,38]. However, quantum chemical calculations suggested another alternative, i.e. a complex with the distal histidine as proton acceptor (δ protonation state, see Fig. 4) [39,40]. In order to shed light into the question which protonation state leads to stronger FeN and H-bonding, we applied the local mode analysis (implying unconstrained geometry optimizations and harmonic frequency calculations with 8664 degrees of freedom) for the myoglobin active site with the distal histidine in the ϵ protonation state, (model **2**) and δ protonation state, (model **3**) compared with gas phase models **1** and **4** shown in Fig. 4. The results are summarized in Table 2.

As revealed by the data in Table 2 the iron-azanone bond is shorter and stronger for the ϵ protonation state than for the δ protonation state (d = 1.754 Åand k^a = 3.125 mDyn/Åcompared with 1.777 Åand 2.708 mDyn/Årespectively). Also the H-bond in the ϵ protonation state is stronger than that in the δ protonation state; (k^a = 0.182 mDyn/Åversus 0.099 mDyn/Å). These results strongly favor the ϵ protonation state in line with the experimental findings. Comparison with gas phase model **1** reveals that the protein environment has the largest influence on the azanone ligand in the ϵ protonation state of the distal histidine, which is further reflected by the azarone NO and NH bonds. In comparison with model **1**, the FeN bonds between Fe and azanone in model **4a** are weakened (k^a is reduced from 2.811 to 1.758) by the presence of the two azanone ligands, whereas in model **4b** the FeN bonds between Fe and histidine are strengthened (k^a is increased from 1.189 to 1.431) by the two histidine ligands.

3.3. Metal-ligand local mode force constants to be used as force field parameters

The local mode analysis can be also used to complement missing force constants in molecular mechanical force fields. Particularly interesting are metal-ligand force constants which are often difficult to estimate [41]. For example, in order to investigate the degradation of toxic organomercuric species catalyzed by the enzyme organomercurial lyase MerB [EC 4.99.1.2] [42] with QM/MM methodologies such as ONIOM [29] one needs suited mercury force field parameters for the molecular mechanics (MM) part. As shown in Fig. 5, the cleavage/formation of Hg-S and Hg-C bonds play a critical role. We derived local mode Hg-S and Hg-C stretching and S-Hg-C bending force constants using methyl(methylthio) mercury as a model compound and determined the corresponding force constants at the NESC/PBE0/def2-TZVPP level of theory [44,45] and utilizing a SARC basis set [46] for Hg. The relativistic NESC method guarantees an accurate description of mercury [47]. The calculated Hg–S and Hg–C bond lengths are 2.335 and 2.083 Å, respectively, and the corresponding local mode force constants are 2.008 and 2.317 mDyn/Å. The S–Hg–C part of methl

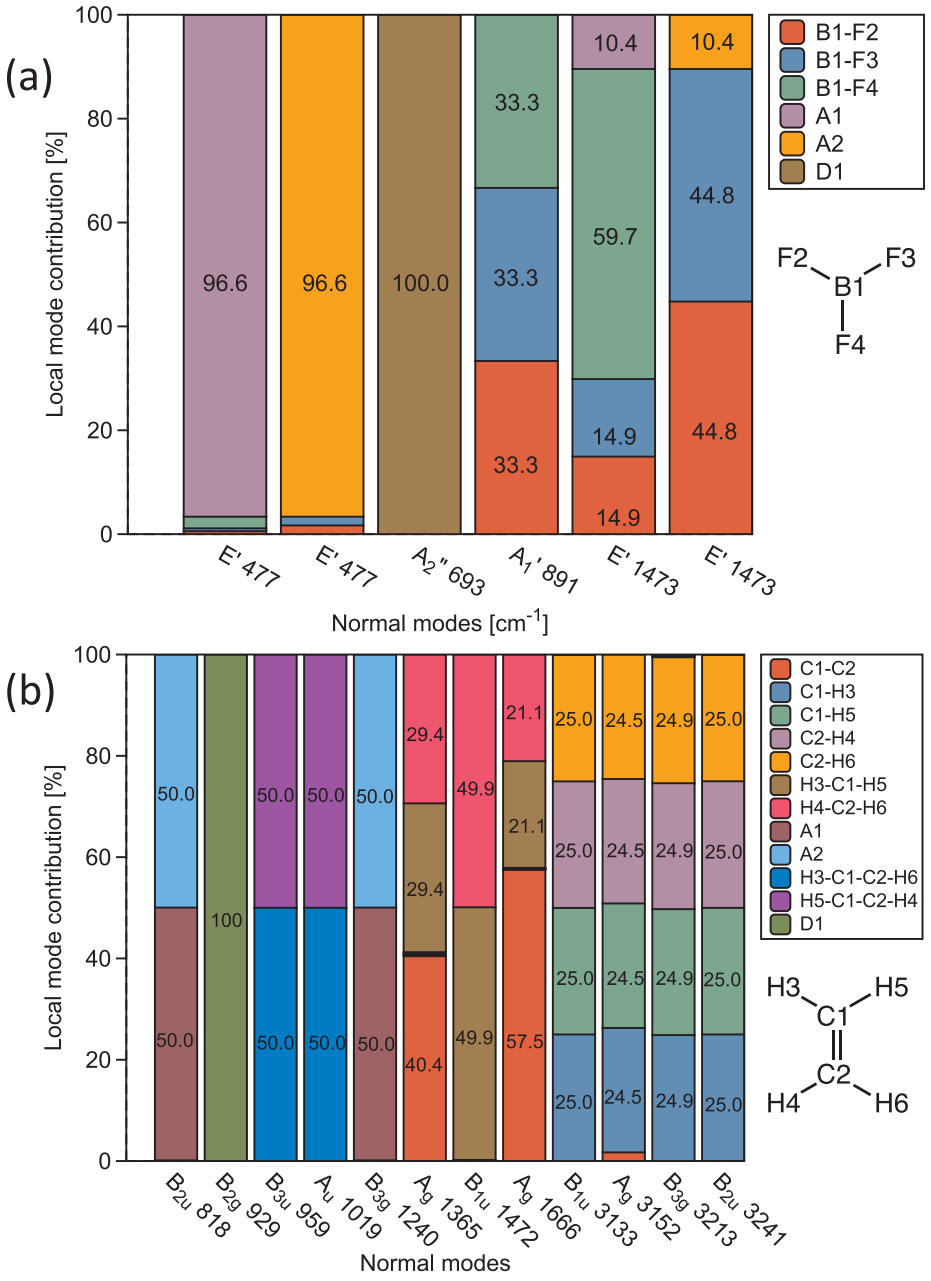

Fig. 3. Decomposition of each normal vibrational mode (presented as a bar) into local mode contributions, (a) for BF_3 and (b) C_2H_4. Under the X-axis the irreducible representation and vibrational frequency (in cm^{-1}) for each normal mode are given. The local modes are color coded as defined in the legend. Figure (a): A1 is the combination of local modes F2-B1-F3 with a contribution of $c_1 = \sqrt{2/3}$, F2-B1-F4 and F3-B1-F4 with a contribution of $-c_1/2$; A2 the combination of F2-B1-F4 with a contribution of $c_2 = \sqrt{1/2}$ and F3-B1-F4 with $-c_2$; D1 the combination of local modes F2-B1-F3-F4, F3-B1-F4-F2, and F4-B1-F2-F3 with a contribution of $c_3 = \sqrt{1/3}$. Figure (b): A1 is the combination of $c_2 \times$ C2-C1-H3 and $-c_2 \times$ C2-C1-H5; A2 the combination of $c_2 \times$ C1-C2-H4 and $-c_2 \times$ C1-C2-H6; D1 the combination of C2-C1-H3-H5 and C1-C2-H4-H6 with an equal contribution of c_2. The combination coefficients c are determined by diagonalizing a $n \times n$ unit-matrix (n: number of equivalent local modes in a specific combination).

(methylthio) mercury is almost linear with a bond angle of 178.5 degree and a corresponding local mode force constant value of 0.406 mDyn·Å/Rad^2. Because of their local nature, these force constants are transferrable and independent on the coordinate system in contrast the to force constants derived from the diagonal elements of the force constant matrix [48] and therefore, are ideally suited as force field parameters. Work is in progress to investigate the complete mercury degradation cycle shown in Fig. 5 at the QM/MM level using the Hg-ligand force constants for the MM part derived in this study, parallel to the compilation of a library with metal-ligand force constants, which we have recently coined metal-ligand electronic parameters MLEP [49,50].

4. Conclusions

In this work we have summarized the theory of local vibrational modes in particular focusing on local mode force constants, their relationship with and advantage over compliance/relaxed force constants. We have demonstrated the large application potential of local mode force constants in three examples. (i) We could unveil the limitation of empirically derived bending force constants by a comparison with high-accuracy CCSD(T)/aug-cc-pVTZ local mode force constants and the decomposition of normal modes into local mode contributions. (ii) We could quantify for the first time the experimental findings that the complex of HNO and myoglobin involves the distal histidine of the

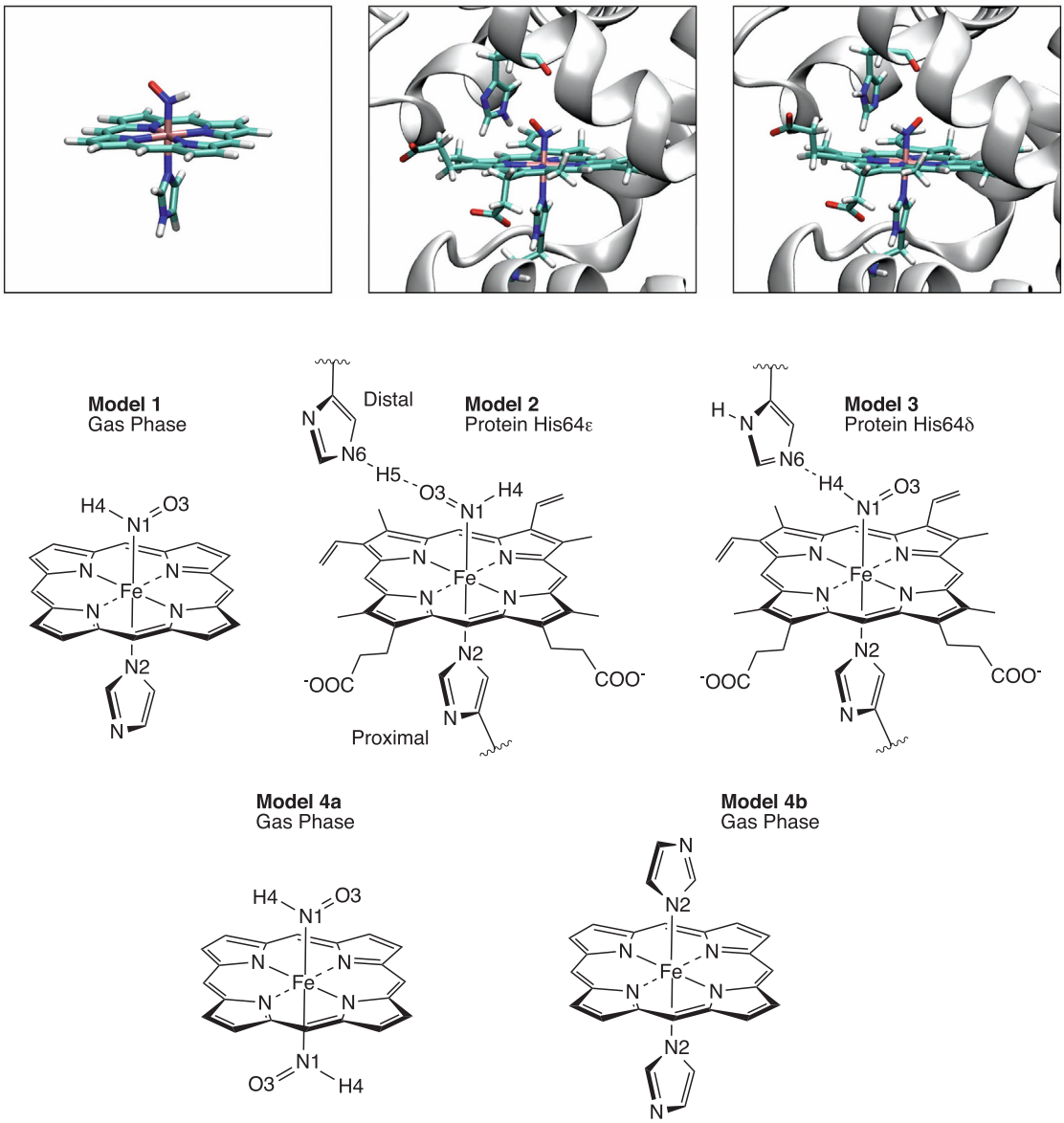

Fig. 4. HNO coordinated to the heme group in the gas phase, Model **1** and **4** and in myoglobin, Model **2** (His64ϵ) and Model **3** (His64δ). Gas phase calculations: PBE0/6-31G(d,p); Protein calculations: QM/MM with PBE0/6-31G(d,p)/AMBER using the ONIOM method with the electronic embedding [29]. Starting protein coordinates were based on modified X-ray data of NO complexed to horse heart myoglobin; [PDB entry: 2FRJ] [35].

heme pocket as proton donor contrary to some computational suggestions. (iii) We introduced mercury-ligand local force constants as potential mercury-ligand force field parameters. We hope that this work will inspire the spectroscopic community and will open the avenue for wide-spread future use of local vibrational force constants.

Table 2
Bond distances *d* and local mode force constants k^a for selected bonds[a] of gas phase models **1**, **4a**, and **4b** (PBE0/6-31G(d,p)) calculations), and myoglobin models **2** and **3**, (ONIOM: PBE0/6-31G(d,p)/AMBER calculations.

	Model **1**		Model **2**		Model **3**		Model **4a**		Model **4b**	
Bond	d (Å)	k^a (mDyn/Å)	d (Å)	k^a (mDyn/Å)	d (Å)	k^a (mDyn/Å)	d (Å)	k^a (mDyn/Å)	d (Å)	k^a (mDyn/Å)
O3···H5	–	–	1.945	0.182	–	–	–	–	–	–
H4···N6	–	–	–	–	2.069	0.099	–	–	–	–
O3–N1	1.215	11.579	1.225	10.944	1.220	11.220	1.206	12.164	–	–
N1–H4	1.045	5.444	1.043	5.561	1.049	5.314	1.047	5.417	–	–
Fe–N1	1.774	2.811	1.754	3.125	1.777	2.708	1.843	1.758	–	–
Fe–N2	2.032	1.189	2.038	1.308	2.053	1.170	–	–	1.983	1.431

[a] For a number of atoms, see Fig. 4.

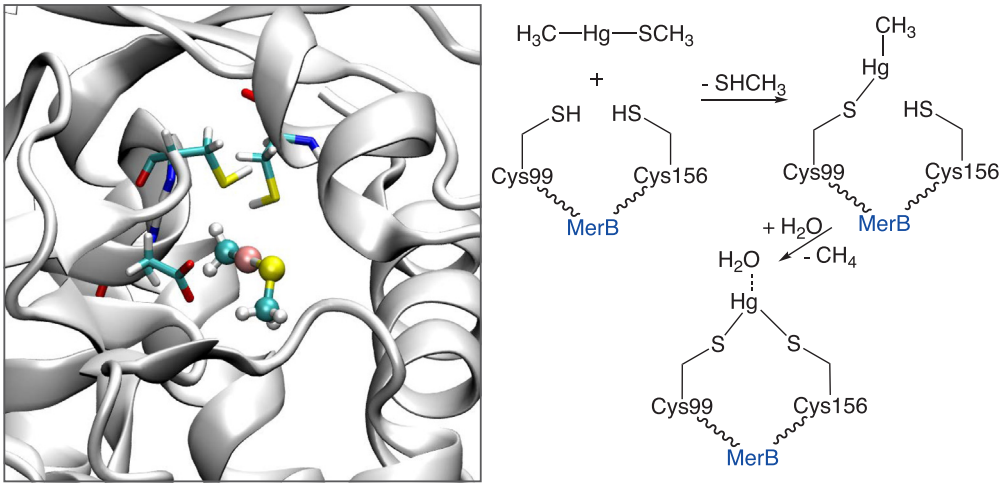

Fig. 5. Left: Methyl(methylthio) mercury substrate inside the active site of the organomercurial lyase MerB based on the X-ray protein structure [43]. Right: Suggested mercury degradation mechanism involving Cys99 and Cys156 of the organomercurial lyase MerB [42].

CRediT authorship contribution statement

Wenli Zou: Methodology, Software, Investigation, Data curation, Writing - original draft, Writing - review & editing, Funding acquisition. **Yunwen Tao:** Methodology, Data curation, Writing - original draft, Writing - review & editing. **Marek Freindorf:** Formal analysis, Data curation, Visualization. **Elfi Kraka:** Conceptualization, Methodology, Writing - review & editing, Supervision, Funding acquisition.

Declaration of Competing Interest

The authors declare that they have no known competing financial interests or personal relationships that could have appeared to influence the work reported in this paper.

Acknowledgements

This work was financially supported by the National Science Foundation, Grants CHE 1152357 and CHE 1464906. We thank SMU for providing computational resources. At Xi'an, this work was supported by the National Natural Science Foundation of China (Grant No. 21673175) and the Double First-Class University Construction Project of Northwest University. We also thank Miss Chun Gao of Northwest University for performing the CFOUR calculations.

Appendix A. Supplementary material

Supplementary data associated with this article can be found, in the online version, at https://doi.org/10.1016/j.cplett.2020.137337.

References

[1] R.M. Badger, A relation between internuclear distances and bond force constants, J. Chem. Phys. 2 (1934) 128–131.
[2] E. Kraka, J.A. Larsson, D. Cremer, Generalization of the Badger rule based on the use of adiabatic vibrational modes, in: J. Grunenberg (Ed.), Computational Spectroscopy, Wiley, New York, 2010, pp. 105–149.
[3] E.B. Wilson, J.C. Decius, P.C. Cross, Molecular Vibrations, McGraw-Hill, New York, 1955.
[4] G. Herzberg, Molecular Spectra and Molecular Structure, II. Infrared and Raman Spectra of Polyatomic Molecules, Van Nostrand, New York, 1945.
[5] J. Decius, Compliance matrix and molecular vibrations, J. Chem. Phys. 38 (1963) 241–248.
[6] L.H. Jones, B.I. Swanson, Interpretation of potential constants: application to study of bonding forces in metal cyanide complexes and metal carbonyls, Acc. Chem. Res. 9 (1976) 128–134.
[7] K. Brandhorst, J. Grunenberg, Efficient computation of compliance matrices in redundant internal coordinates from cartesian hessians for nonstationary points, J. Chem. Phys. 132 (2010) 184101.
[8] Z. Konkoli, J.A. Larsson, D. Cremer, A new way of analyzing vibrational spectra. II. Comparison of internal mode frequencies, Int. J. Quant. Chem. 67 (1998) 11–27.
[9] Z. Konkoli, J.A. Larsson, D. Cremer, A new way of analyzing vibrational spectra. IV. Application and testing of adiabatic modes within the concept of the characterization of normal modes, Int. J. Quant. Chem. 67 (1998) 41–55.
[10] W. Zou, R. Kalescky, E. Kraka, D. Cremer, Relating normal vibrational modes to local vibrational modes with the help of an adiabatic connection scheme, J. Chem. Phys. 137 (2012) 084114.
[11] W. Zou, D. Cremer, C_2 in a box: determining its intrinsic bond strength for the $X\,^1\Sigma_g^+$ ground state, Chem. Eur. J. 22 (2016) 4087–4097.
[12] W. Zou, D. Cremer, Properties of local vibrational modes: the infrared intensity, Theor. Chem. Acc. 133 (2014) 1451–1466.
[13] W. Zou, R. Kalescky, E. Kraka, D. Cremer, Relating normal vibrational modes to local vibrational modes: benzene and naphthalene, J. Mol. Model. 19 (2012) 2865–2877.
[14] Z. Konkoli, D. Cremer, A new way of analyzing vibrational spectra. I. Derivation of adiabatic internal modes, Int. J. Quant. Chem. 67 (1998) 1–9.
[15] W. Zou, D. Izotov, D. Cremer, New way of describing static and dynamic deformations of the Jahn-Teller type in ring molecules, J. Phys. Chem. A 115 (2011) 8731–8742.
[16] L. Burnelle, C.A. Coulson, Bond dipole moments in water and ammonia, Trans. Faraday Soc. 53 (1957) 403–405.
[17] D.R. Borst, T.M. Korter, D.W. Pratt, On the additivity of bond dipole moments. Stark effect studies of the rotationally resolved electronic spectra of aniline, benzonitrile, and aminobenzonitrile, Chem. Phys. Lett. 350 (2001) 485–490.
[18] J.-S. Cao, M.-J. Wei, F.-W. Chen, Relationship between the bond dipole moment and bond angle of polar molecules, Acta Phys.-Chim. Sin. 32 (2016) 1639–1648.
[19] C.F. Jackels, Z. Gu, D.G. Truhlar, Reaction-path potential and vibrational frequencies in terms of curvilinear internal coordinates, J. Chem. Phys. 102 (8) (1995) 3188–3201.
[20] J.W. Ochterski, Vibrational Analysis in Gaussian, 1999, http://gaussian.com/vib/ (accessed on May 5, 2018).
[21] K. Raghavachari, G.W. Trucks, J.A. Pople, M. Head-Gordon, A fifth-order perturbation comparison of electron correlation theories, Chem. Phys. Lett. 157 (1989) 479–483.
[22] CFOUR Ver. 2.00β, Coupled-Cluster techniques for Computational Chemistry, a quantum-chemical program package by J.F. Stanton, J. Gauss, M.E. Harding, P.G. Szalay with contributions from A.A. Auer, R.J. Bartlett, U. Benedikt, C. Berger, D.E. Bernholdt, Y.J. Bomble, L. Cheng, O. Christiansen, M. Heckert, O. Heun, C. Huber, T.-C. Jagau, D. Jonsson, J. Jusélius, K. Klein, W.J. Lauderdale, F. Lipparini, D.A. Matthews, T. Metzroth, L.A. Mück, D.P. O'Neill, D.R. Price, E. Prochnow, C. Puzzarini, K. Ruud, F. Schiffmann, W. Schwalbach, C. Simmons, S. Stopkowicz, A. Tajti, J. Vázquez, F. Wang, J.D. Watts and the integral packages MOLECULE (J. Almlöf and P.R. Taylor), PROPS (P.R. Taylor), ABACUS (T. Helgaker, H.J. Aa. Jensen, P. Jørgensen, and J. Olsen), and ECP routines by A.V. Mitin and C. van Wüllen, 2014. For the current version, see http://www.cfour.de (accessed on May 5, 2018).
[23] G.E. Scuseria, Analytic evaluation of energy gradients for the singles and doubles coupled cluster method including perturbative triple excitations: Theory and applications to FOOF and Cr_2, J. Chem. Phys. 94 (1991) 442–447.
[24] J. Gauss, J.F. Stanton, Analytic CCSD(T) second derivatives, Chem. Phys. Lett. 276 (1997) 70–77.
[25] M.J. Frisch, G.W. Trucks, H.B. Schlegel, G.E. Scuseria, M.A. Robb, J.R. Cheeseman, G. Scalmani, V. Barone, G.A. Petersson, H. Nakatsuji, X. Li, M. Caricato, A.V. Marenich, J. Bloino, B.G. Janesko, R. Gomperts, B. Mennucci, H.P. Hratchian, J.V. Ortiz, A.F. Izmaylov, J.L. Sonnenberg, D. Williams-Young, F. Ding, F. Lipparini, F. Egidi, J. Goings, B. Peng, A. Petrone, T. Henderson, D. Ranasinghe, V.G.

Zakrzewski, J. Gao, N. Rega, G. Zheng, W. Liang, M. Hada, M. Ehara, K. Toyota, R. Fukuda, J. Hasegawa, M. Ishida, T. Nakajima, Y. Honda, O. Kitao, H. Nakai, T. Vreven, K. Throssell, J.A. Montgomery Jr., J.E. Peralta, F. Ogliaro, M.J. Bearpark, J. J. Heyd, E.N. Brothers, K.N. Kudin, V.N. Staroverov, T.A. Keith, R. Kobayashi, J. Normand, K. Raghavachari, A.P. Rendell, J.C. Burant, S.S. Iyengar, J. Tomasi, M. Cossi, J.M. Millam, M. Klene, C. Adamo, R. Cammi, J.W. Ochterski, R.L. Martin, K. Morokuma, O. Farkas, J.B. Foresman, D.J. Fox, Gaussian16 Revision B.01, gaussian Inc., Wallingford CT, 2016.

[26] E. Kraka, W. Zou, M. Filatov, Y. Tao, J. Grafenstein, D. Izotov, J. Gauss, Y. He, A. Wu, Z. Konkoli, V. Polo, L. Olsson, Z. He, D. Cremer, COLOGNE2019, 2019, see http://www.smu.edu/catco.

[27] B.P. Pritchard, D. Altarawy, B. Didier, T.D. Gibson, T.L. Windus, New basis set exchange: an open, up-to-date resource for the molecular sciences community, J. Chem. Inf. Model. 59 (11) (2019) 4814–4820.

[28] EMSL Basis Set Exchange. Available at: https://www.basissetexchange.org/ (accessed on June 10, 2019).

[29] L.W. Chung, W.M.C. Sameera, R. Ramozzi, A.J. Page, M. Hatanaka, G.P. Petrova, T.V. Harris, X. Li, Z. Ke, F. Liu, H.-B. Li, L. Ding, K. Morokuma, The ONIOM method and its applications, Chem. Rev. 115 (12) (2015) 5678–5796.

[30] D.A. Case, I.Y. Ben-Shalom, S.R. Brozell, D.S. Cerutti, T.E. Cheatham, V.W.D. Cruzeiro, T.A. Darden, R.E. Duke, D. Ghoreishi, M.K. Gilson, H. Gohlke, A.W. Goetz, D. Greene, R. Harris, N. Homeyer, S. Izadi, A. Kovalenko, T. Kurtzman, T.S. Lee, S. LeGrand, P. Li, C. Lin, J. Liu, T. Luchko, R. Luo, D.J. Mermelstein, K.M. Merz, Y. Miao, G. Monard, C. Nguyen, H. Nguyen, I. Omelyan, A. Onufriev, F. Pan, R. Qi, D. R. Roe, A. Roitberg, C. Sagui, S. Schott-Verdugo, J. Shen, C.L. Simmerling, J. Smith, R. Salomon-Ferrer, J. Swails, R.C. Walker, J. Wang, H. Wei, R.M. Wolf, X. Wu, L. Xiao, D.M. York, P.A. Kollman, AMBER, 2018.

[31] R.P. Bell, The occurrence and properties of molecular vibrations with $V(x) = ax^4$, Proc. Roy. Soc. 183 (1945) 328–337.

[32] W. Gordy, A relation between bond force constants, bond orders, bond lengths, and the electronegativities of the bonded atoms, J. Chem. Phys. 14 (1946) 305–320.

[33] Z. Konkoli, D. Cremer, A new way of analyzing vibrational spectra. III. Characterization of normal vibrational modes in terms of internal vibrational modes, Int. J. Quant. Chem. 67 (1998) 29–40.

[34] D. Cremer, J.A. Larsson, E. Kraka, New developments in the analysis of vibrational spectra on the use of adiabatic internal vibrational modes, in: C. Parkanyi (Ed.), Theoretical and Computational Chemistry, Elsevier, Amsterdam, 1998, pp. 259–327.

[35] D.M. Copeland, A.S. Soares, A.H. West, G.B. Richter-Addo, Crystal structures of the nitrite and nitric oxide complexes of horse heart myoglobin, J. Inorg. Biochem. 100 (8) (2006) 1413–1425.

[36] H.-J. Sun, W.-T. Lee, B. Leng, Z.-Y. Wu, Y. Yang, J.-S. Bian, Nitroxyl as a potential theranostic in the cancer arena, Antioxid. Redox Sign. 32 (2019) 331–349.

[37] F. Sulc, C.E. Immoos, D. Pervitsky, P.J. Farmer, Efficient trapping of HNO by deoxymyoglobin, J. Am. Chem. Soc. 126 (4) (2004) 1096–1101.

[38] C.E. Immoos, F. Sulc, P.J. Farmer, K. Czarnecki, D.F. Bocian, A. Levina, J.B. Aitken, R.S. Armstrong, P.A. Lay, Bonding in HNO-myoglobin as characterized by X-ray absorption and resonance raman spectroscopies, J. Am. Chem. Soc. 127 (3) (2005) 814–815.

[39] L. Yang, Y. Ling, Y. Zhang, HNO binding in a heme protein: Structures, spectroscopic properties, and stabilities, J. Am. Chem. Soc. 133 (2011) 13814–13817.

[40] R.L. Khade, Y. Yang, Y. Shi, Y. Zhang, HNO-binding in heme proteins: effects of iron oxidation state, axial ligand, and protein environment, Angew. Chem. Int. Ed. 55 (48) (2016) 15058–15061.

[41] P.C. abd Bodo Martin, Molecular modeling of transition metal and rare earth coordination compounds, Adv. Inorg. Chem. 73 (2019) 305–321.

[42] P.J. Silva, V. Rodrigues, Mechanistic pathways of mercury removal from the organomercurial lyase active site, PeerJ 3 (2015) e1127-1–e1127-18.

[43] J. Lafrance-Vanasse, M. Lefebvre, P. Di Lello, J. Sygusch, J.G. Omichinski, Crystal structures of the organomercurial lyase MerB in its free and mercury-bound forms: Insights into the mechanism of methylmercury degradation, J. Biol. Chem. 284 (2) (2009) 938–944.

[44] C. Adamo, V. Barone, Toward reliable density functional methods without adjustable parameters: the PBE0 model, J. Chem. Phys. 110 (13) (1999) 6158–6170.

[45] F. Weigend, R. Ahlrichs, Balanced basis sets of split valence, triple zeta valence and quadruple zeta valence quality for H to Rn: Design and assessment of accuracy, Phys. Chem. Chem. Phys. 7 (18) (2005) 3297–3305.

[46] D.A. Pantazis, X.-Y. Chen, C.R. Landis, F. Neese, All-electron scalar relativistic basis sets for third-row transition metal atoms, J. Chem. Theory Comput. 4 (6) (2008) 908–919.

[47] D. Cremer, W. Zou, M. Filatov, Dirac-exact relativistic methods: the normalized elimination of the small component method, WIREs Comput. Mol. Sci. 4 (2014) 436–467.

[48] G. Fogarasi, P. Pulay, Ab initio vibrational force fields, Annual Rev. Phys. Chem. 35 (1984) 191–213.

[49] D. Cremer, E. Kraka, Generalization of the Tolman electronic parameter: the metal-ligand electronic parameter and the intrinsic strength of the metal-ligand bond, Dalton Trans. 46 (2017) 8323–8338.

[50] M.Z. Makoś, M. Freindorf, D. Sethio, E. Kraka, New insights into Fe-H2 and Fe-H-bonding of a [NiFe] hydrogenase mimic – a local vibrational mode study, Theor. Chem. Acc. 138 (2019) 76-1–76-18.